



Thermodynamic selection criteria of zeotropic mixtures for subcritical organic Rankine cycle

Zheng Miao, Kai Zhang, Mengxiao Wang, Jinliang Xu*

The Beijing Key Laboratory of Multiphase Flow and Heat Transfer for Low Grade Energy Utilization, North China Electric Power University, Beijing, 102206, PR China

ARTICLE INFO

Article history:

Received 18 April 2018
Received in revised form
26 September 2018
Accepted 2 November 2018
Available online 4 November 2018

Keywords:

Organic Rankine cycle
Zeotropic mixtures
Temperature match
Selection criteria
Exergy analysis

ABSTRACT

Although using zeotropic mixtures in the organic Rankine cycle (ORC) system can improve its performance, the selection of the mixture working fluid is still a great challenge due to the lack of selection criteria. In the present work, the thermodynamic selection criteria of zeotropic mixtures is proposed based on the exergy analysis of the subcritical ORC. The mixture composition can be directly determined according to the thermophysical properties of working fluids without massive thermodynamic calculation. The effect of temperature match between the working fluids and the heat source/sink on the system performance is analyzed. And the overall exergy efficiency is set as the optimization index. For the heat source without limit to the outlet temperature, the improvement of the temperature match in the evaporator exhibits more significant influence on the cycle performance than that in the condenser. Thus, the match condition with the heat source should be firstly satisfied when selecting working fluids. The proper temperature glide in the condenser can further improve the cycle performance. The 'wet' mixtures have relatively lower cycle performance compare to 'dry' and 'isotropic' ones. The steps of using this selection criteria and a case study to validate it are also illustrated.

© 2018 Elsevier Ltd. All rights reserved.

1. Introduction

Increasing concerns over energy shortage and environment pollution are leading to a surge of interest in utilization of low grade energy. Organic Rankine cycle (ORC) use low boiling point organic fluids to convert low temperature heat to work, and is regarded as a promising technology in the future [1–5].

Currently, the efficiency of ORC system driven by low temperature heat is still low. The exergy destruction in heat transfer processes contributes the largest part of irreversible losses of an ORC system [6]. Zeotropic mixture presents a temperature glide during the phase change, which can provide a better temperature match between the working fluid and heat source/sink, consequently, reducing the irreversible losses. Thus, using zeotropic mixtures as working fluids has been paid more and more attentions [7]. Various pure organic fluid can be used in the ORC, and the number of their mixtures is much more. The selection of a mixture working fluid involves not only the selection of the suitable components but also

the determination of the optimal concentration. This results in a tremendous computing workload and poses a great challenge for the selection of working fluid. So the working fluid selection criterion related to its thermophysical properties is essential to carry out a simple and rapid preliminary selection of working fluids without massive calculation.

Working fluid selection is an important aspect of the ORC research. At present, pure working fluids have been widely investigated. It is generally believed that the critical temperature of working fluids and the inlet temperature of heat source exhibited a significant effect on the cycle performance. Several selection criteria were proposed based on these two parameters [8–19]. Some scholars believed that the optimal critical temperature should be 33 K [13] or 30–50 K [15] lower than the heat source inlet temperature, while others claimed that the optimal critical temperature should be 0.8 times of the heat source inlet temperature [18] or a linear relationship with the heat source inlet temperature [19].

In recent years, studies on the selection of mixture working fluid has been increasing. Bao et al. [20] and Bamorovat et al. [21] reviewed former works on the mixtures as working fluids in the ORC, and summarized that the improvement of the system

* Corresponding author.

E-mail address: xjl@ncepu.edu.cn (J. Xu).

performance was mainly a consequence of the optimized temperature match in the condenser. Most scholars focused on analyzing the effects of operation conditions, mixture composition on system performance and the temperature match between mixtures and cooling fluids, so as to find the suitable working fluid [22–35]. A few scholars carried out the thermoeconomic comparisons between pure and mixture working fluids [36–39]. Chys et al. [22] found that the mixture composition corresponding to the maximum temperature glide could deliver the optimal temperature match, and a potential increase of 16% and 6% in cycle efficiency could be achieved by using zeotropic mixtures as working fluids at 150 °C and 250 °C heat sources. Heberle et al. [23] studied the performance of an ORC system using isobutane/isopentane and R227ea/R245fa and found that the raise of the second law efficiency was up to 15% for mixtures compared to pure fluids. If the pinch point moved to the preheater inlet, there was a significant efficiency increase. And the suitable mixtures should give a condensation temperature glide fitting with temperature difference of the cooling water. The same conclusion was obtained from the work of Liu et al. [24]. They also found that when two optimal working fluid mole fractions occurred, the highest net power output appeared at the higher mole fraction of the more volatile component. Lecompte et al. [25] analyzed the thermodynamic performance of subcritical ORC with mixtures as working fluids based on the second law analysis. The results showed that the reason of system performance improvement using mixtures lied in a combination of higher heat input in the evaporator and less exergy loss in the condenser, and the optimal condensation temperature glide slope was slightly smaller than the glide slope of the cooling fluid. Zhou et al. [27] presented a performance analysis of zeotropic mixtures for the dual-loop system and also found that appropriate mixtures improved not only the thermal efficiency but also the absorbed heat from heat source because of better temperature match in the condensation process. Song et al. [30] used the net power output and second law efficiency as the criteria to select the suitable working fluid compositions and they claimed that using mixtures instead of pure fluids provided better temperature matches with the heat source and sink, thereby reducing the exergy loss of the heat transfer process. Dong et al. [32] investigated the performance of an ORC system using MM/MDM as working fluids for the heat source with 280 °C inlet temperature and 240 °C outlet temperature and found that the non-isothermal phase transition gradient led to lower irreversibility rates of evaporator and condenser. MM/MDM(0.4/0.6, mass) showed the best performance. Andreasen et al. [33] studied the temperature match between mixtures and the cooling fluid at the fixed heat source inlet temperatures of 120 °C and 90 °C. Their results indicated that the mixtures composed of the fluids with the large difference between boiling points had a non-linear temperature glide and were therefore not able to match the temperature profile of the cooling water when the condensation temperature glide closed to the temperature increase of the cooling water.

Recently, it is a hot spot in the research of halohydrocarbons as the flame retardants and blending with hydrocarbons to form zeotropic mixtures [28–30]. Kang et al. [28] suggested that R245fa/R600a (0.9/0.1, mass) was the most preferable mixture among the working fluids within the research scope for the ORC with 110 °C heat source. Shu et al. [29] found that there existed the optimal concentration corresponding to the highest thermal efficiency for different mixtures, and it gradually approached the side of fewer retardants with the increase of evaporation temperature. Some scholars believed that the condensation temperature glide of mixtures lowered the ORC thermodynamic performance at a fixed condensation bubble point temperature, while improved cycle performance at a fixed condensation dew point temperature

[26,34]. In addition, some nonlinear optimization solvers are used to select mixtures. By solving Mixed-Integer Nonlinear Programming (MINLP), Magdalena et al. [40] put forward a nonlinear stochastic optimization method to design the composition of mixture capable of withstanding variability in heat source temperatures and efficiencies of expander. Bao et al. [41] introduced a selective coefficient to represent the component alternative and proposed a method to select the optimal components and compositions of zeotropic mixture at the same time.

Most researches of the ORC using zeotropic mixtures mainly focus on the optimization of temperature match in the condenser, and recommend the suitable mixture composition for the specific heat source. Only a few scholars considered the temperature match between the working fluid and heat source/sink at the same time. It is noted that the temperature match in the evaporator exhibits a significant effect on the ORC performance when there is no limitation on the heat source outlet temperature. Zhao et al. [42] performed the thermodynamic analysis of the ORC system using zeotropic mixtures. It is found that the heat source inlet temperature showed a prominent influence on the composition of zeotropic mixtures when other working conditions were constant. Braimakis et al. [43] performed a simulation for heat source temperatures ranging from 150 to 300 °C, and they found that there was a positive correlation between the optimal heat source temperature and working fluid critical temperature. In addition, when the temperature glide approaches the cooling water temperature difference in the condensation process, the exergy efficiency can be improved. Therefore, they concluded that their optimal component ratio for maximizing the exergy efficiency depends on the combined influence of these two effects. Andreasen et al. [33] considered the optimal critical temperature is close to half of the heat source inlet temperature, while Hærving et al. [15] believed the optimal critical temperature is approximately 30–50 K below the hot source. They all presented that optimal mixture can be found when the condensation temperature glide matches the temperature increase of the cooling water. By treating the zeotropic mixture as a pure working fluid with adjustable temperature glide, Zhai et al. [44] proposed an active design method of the zeotropic mixture for the open type heat source (without outlet temperature limitation), considering the relationships between the working fluid and heat source/sink.

From the review of literature above, it can be summarized that the selection of mixture working fluids for ORC system is still a great challenge due to the massive thermodynamic calculation and blind trials. It is necessary to build a simple and practicable selection criteria of mixture working fluids so that some suitable mixture compositions can be preliminary screened directly and rapidly from a large number of pure working fluids. In the meanwhile, how non-isothermal phase change process of zeotropic mixtures influencing the ORC system thermodynamic performance need to be further studied. In this paper, a selection criteria of mixture working fluids for the ORC system using heat source without outlet temperature limitation is proposed. The criteria is based on two quantitative correlations describing the required temperature match in the evaporator and condenser for the suitable mixture. Consequently, the mixture components and concentration can be determined directly according to the thermophysical properties of working fluids without massive calculation. The overall exergy efficiency is used as the optimization objective in the thermodynamic analysis. The influence of mixture temperature glide during phase change on the overall exergy efficiency is analyzed. And a case study is carried out to validate the selection criteria.

2. Model description

Fig. 1 shows the schematic diagram of a basic subcritical ORC system. The liquid working fluid is pumped to the evaporator to be gasified by the heat source. Then, the high temperature and pressure vapor flows into the expander to generate work. The low pressure exhaust is cooled and condensed into liquid in the condenser and goes to the pump beginning a new cycle.

2.1. Assumptions of the model for ORC system using mixtures

- (1) The system is under the steady state.
- (2) Heat loss and pressure drop in the heat exchangers and pipes are ignored.
- (3) The concentration of mixtures is constant in cycle.
- (4) The potential and kinetic energy of the working fluids are ignored.
- (5) The heat exchanger is a counter flow layout.

2.2. First law of the thermodynamic analysis

The T - s diagram of the subcritical ORC system using mixtures is shown in Fig. 2. Corresponding to the number in Fig. 2, the expressions of key variables are given as follows.

The heat load of the evaporator:

$$\dot{Q}_{hs} = \dot{m}_{wf}(h_1 - h_6) = \dot{m}_{hs}(h_9 - h_{10}) \quad (1)$$

The shaft power of the expander:

$$\dot{W}_{exp} = \dot{m}_{wf}(h_1 - h_2) = \eta_{exp}\dot{m}_{wf}(h_1 - h_{2s}) \quad (2)$$

The work consumed by the pump:

$$\dot{W}_{pump} = \dot{m}_{wf}(h_6 - h_5) = \frac{\dot{m}_{wf}(h_{6s} - h_5)}{\eta_{pump}} \quad (3)$$

Thus, the net work output is:

$$\dot{W}_{net} = \dot{W}_{exp} - \dot{W}_{pump} \quad (4)$$

And the thermal efficiency is given as:

$$\eta_l = \frac{\dot{W}_{net}}{\dot{Q}_{hs}} \quad (5)$$

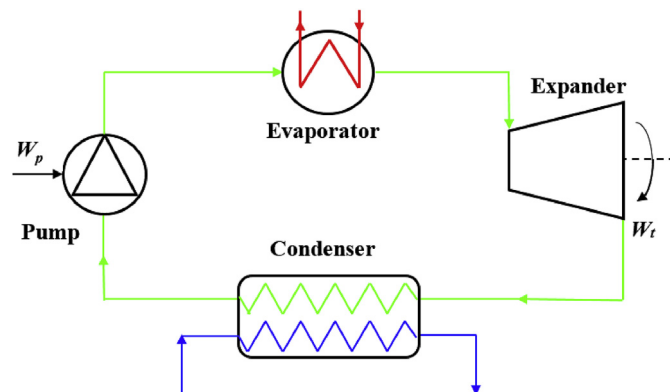


Fig. 1. Schematic diagram of the basic ORC.

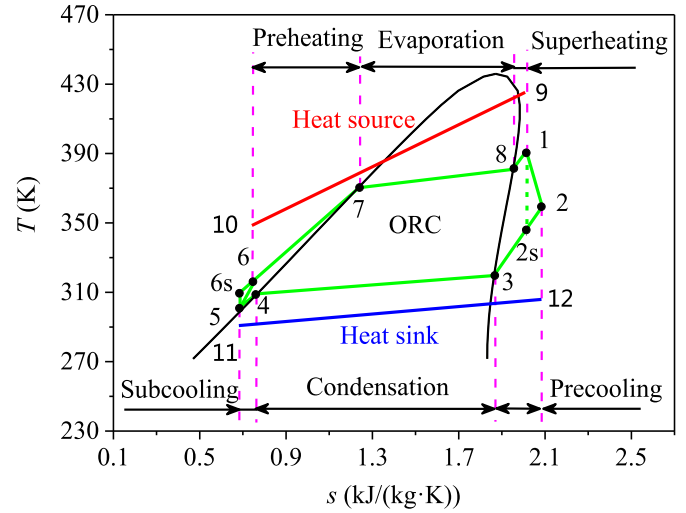


Fig. 2. T - s diagram of the subcritical ORC.

2.3. Second law of the thermodynamic analysis

In the second law analysis, the reference environment state is chosen as $T_0 = 293.15\text{K}$ and $P_0 = 101.325\text{kPa}$. Based on the concept of exergy flow, the heat source inlet exergy is:

$$\dot{E}_{hs} = \dot{m}_{hs}(h_9 - h_0 - T_0(s_9 - s_0)) \quad (6)$$

And the exergy released by the heat source in the evaporator is:

$$\Delta\dot{E}_{hs} = \dot{m}_{hs}(h_9 - h_{10} - T_0(s_9 - s_{10})) \quad (7)$$

Consequently, the heat source exergy loss (the unused exergy of the heat source) is calculated by:

$$\dot{I}_{hs} = \dot{E}_{hs} - \Delta\dot{E}_{hs} = \dot{m}_{hs}(h_{10} - h_0 - T_0(s_{10} - s_0)) \quad (8)$$

The exergy absorbed by the working fluid in the evaporator is:

$$\Delta\dot{E}_{wf_abs} = \dot{m}_{wf}(h_1 - h_6 - T_0(s_1 - s_6)) \quad (9)$$

Thus, the exergy loss in the evaporator is given as:

$$\dot{I}_{eva} = \Delta\dot{E}_{hs} - \Delta\dot{E}_{wf_abs} = T_0(\dot{m}_{wf}(s_1 - s_6) - \dot{m}_{hs}(s_9 - s_{10})) \quad (10)$$

The exergy loss in the expander is:

$$\dot{I}_{exp} = T_0\dot{m}_{wf}(s_2 - s_{2s}) \quad (11)$$

The exergy loss in the working fluid pump is:

$$\dot{I}_{pump} = T_0\dot{m}_{wf}(s_6 - s_{6s}) \quad (12)$$

Similar to the heat exchange process in the evaporator, the exergy released by the working fluid in the condenser is:

$$\Delta\dot{E}_{wf_rel} = \dot{m}_{wf}(h_2 - h_5 - T_0(s_2 - s_5)) \quad (13)$$

And the exergy absorbed by the cooling fluid in the condenser is:

$$\Delta\dot{E}_{cf} = \dot{m}_{cf}(h_{12} - h_{11} - T_0(s_{12} - s_{11})) \quad (14)$$

Thus, the exergy loss of the condenser can be calculated by:

$$\dot{I}_{\text{con}} = \Delta \dot{E}_{\text{wf_rel}} - \Delta \dot{E}_{\text{cf}} = T_0 (\dot{m}_{\text{cf}}(s_{12} - s_{11}) - \dot{m}_{\text{wf}}(s_2 - s_5)) \quad (15)$$

Besides, the cooling fluid exergy loss (the unused exergy of the cooling fluid) is also considered and calculated from:

$$\dot{I}_{\text{cf}} = \dot{m}_{\text{cf}}(h_{12} - h_0 - T_0(s_{12} - s_0)) \quad (16)$$

It is noted that, in this work, the coefficient of exergy loss in each process is defined as:

$$\xi_i = \frac{\dot{I}_i}{\dot{E}_{\text{hs}}} \quad (17)$$

where \dot{E}_{hs} is the heat source inlet exergy, given in Eq. (6).

Finally, the overall exergy efficiency is defined as [45,46]:

$$\eta_{\text{II}} = \frac{\dot{W}_{\text{net}}}{\dot{E}_{\text{hs}}} = 1 - \sum \xi_i \quad (18)$$

where η_{II} is directly related to the net work output of the ORC system for a specified heat source as \dot{E}_{hs} is determined by the heat source inlet temperature. The overall exergy efficiency η_{II} reflects the capacity of the cycle to utilize the heat source to do work. It is used as the optimize index in the present thermodynamic analysis.

2.4. Calculation method and condition

The inlet and outlet of exchangers are specified according to the flow direction of working fluids, as shown in Fig. 1. In thermodynamic analysis, the position of the pinch point needs to be determined in the evaporator and condenser. Thus, the heat transfer process is divided into three sections: the liquid section, the two-phase section and the vapor section, shown in Fig. 2. And these three heat transfer section are further discretized into small cells. Based on the energy conservation equation for each cell, the temperature profiles of the working fluid and heat source/sink can be calculated. Thereupon, the minimum temperature difference can be obtained. Iteration is needed to update the evaporation pressure and the condenser pressure to make the minimum temperature difference approach the specified pinch temperature difference. Considering the dry, wet or isentropic behavior of the working fluids, the minimum superheat degree at the expander inlet is defined as the minimum integer value to guarantee the restrictive condition that there is no droplet entrainment at the exit of the expander. Then the cycle operation parameters can also be determined. And the optimal evaporation pressure corresponding to the maximum exergy efficiency can be achieved.

Table 1
Calculation conditions of the model.

Parameter	Symbol	Value	Reference
Expander isentropic efficiency	η_{exp}	0.8	[48,49]
Pump isentropic efficiency	η_{pump}	0.75	[47,48]
Pinch temperature difference in the evaporator	$T_{\text{p,eva}}$	10 K, 20 K and 30 K	[15,19,26]
Pinch temperature difference in the condenser	$T_{\text{p,con}}$	10 K	[16,25]
Superheat degree in the expander inlet	ΔT_{sup}	Minimum	
Subcooling degree in the condenser output	ΔT_{sub}	0 K, 5 K and 10 K	
Heat carrier medium	hs	Air	
Heat source inlet temperature	T_{hs}	393.15 K - 623.15 K	
Heat source fluid mass flow rate	\dot{m}_{hs}	10 kg/s	[26]
Inlet temperature of cooling water	$T_{\text{cf,in}}$	293.15 K	
Outlet temperature of cooling water	$T_{\text{cf,out}}$	303.15 K	

The outlet temperature of the heat source is not limited. The upper pressure limit of the evaporation pressure is set as 90% of the working fluid critical pressure to ensure the stable and safe operation in subcritical region [25,44]. The other operation conditions are listed in Table 1 [15,16,19,25,26,47–49]. The thermodynamic model is developed in the Matlab environment, and the properties of the working fluid are obtained from the Refprop database software [50]. In refprop 9.0, the properties of mixture without corresponding experimental data are estimated by a modified Helmholtz equation [51].

3. Results and discussion

The studied working fluids in the present work are limited to binary zeotropic mixtures. The range of their critical temperature and pressure are listed in Table 2 and Table 3. The pure fluid with lower critical temperature is used as the first part of the mixture's name. Mixtures in Table 2 are all alkane mixtures and their thermophysical properties can be obtained accurately in the software Refprop 9.0. And the "*" symbol in Table 3 means that no corresponding mixture experimental data is available and the mixing parameters are estimated by a modified Helmholtz equation in the Refprop 9.0 database. Thus, in the present work, the selection criteria of mixture working fluid are explored based on alkane mixtures in Table 2, and then verified by mixtures in Table 3.

3.1. Temperature match between the working fluid and heat source

In this section, the subcooling degree is set zero to analyze the effect of the temperature match in the evaporator on the system performance in detail. And the first correlation of the selection criteria is explored.

Table 2
Properties of alkane mixtures used for data fitting (mass fraction 0.0–1.0).

Working fluid	$T_{\text{cri}}(\text{K})$	$P_{\text{cri}}(\text{MPa})$
propane/isobutane	369.89–407.81	3.63–4.33
propane/butane	369.89–425.13	3.8–4.38
isobutene/isopentane	407.81–460.35	3.38–3.75
isobutene/pentane	407.81–469.7	3.37–3.82
butane/isopentane	425.13–460.35	3.38–3.8
butane/pentane	425.13–469.7	3.37–3.81
isopentane/hexane	460.35–507.82	3.03–3.41
pentane/hexane	469.7–507.82	3.03–3.37
hexane/heptane	507.82–540.13	2.74–3.03
heptane/octane	540.13–569.32	2.5–2.74
octane/nonane	569.32–594.55	2.28–2.5

Table 3
Properties of mixtures used for verification (mass fraction 0.0–1.0).

Working fluid	$T_{\text{cri}}(\text{K})$	$P_{\text{cri}}(\text{MPa})$
SF6/R227ea ^(a)	318.72–374.9	2.93–3.75
R125/R22	339.17–369.3	3.62–4.99
R218/R236fa ^(a)	345.02–398.07	2.64–3.2
R22/R152a	369.3–386.41	4.52–4.99
R152a/R142b	386.41–410.26	4.06–4.52
RC318/R245fa ^(a)	388.38–427.16	2.78–3.66
R142b/R141b	410.26–477.5	4.06–4.42
R114/R113	418.83–487.21	3.26–3.62
R365mfc/hexane ^(a)	460–507.82	3.03–3.27

^a No corresponding mixture experimental data is available and the mixing parameters are estimated by a modified Helmholtz equation in the Refprop 9.0 database.

3.1.1. Effect of the heat source inlet temperature and critical temperature

The heat source inlet temperature and the critical temperature of mixture working fluid have a significant influence on the heat transfer process in the evaporator and the performance of the ORC system. As the critical temperature of a mixture varies with its concentration, compared with pure working fluids, the temperature match between the mixture working fluids and the heat source becomes more complicated. So, effect of the heat source inlet temperature and critical temperature is studied for $T_{\text{p,eva}} = 10 \text{ K}$. Fig. 3 shows the effect of the heat source inlet temperature on the overall exergy efficiency at different concentration of the mixture butane/pentane. The critical temperature of butane/pentane varies from 425.13 K to 469.7 K with the mass fraction of pentane increasing from 0.0 to 1.0. It is seen that, when the heat source inlet temperature is lower (423.15 K and 443.15 K), the overall exergy efficiency in the range of butane mass fraction 0.3 to 0.8 is higher. In this case, the results agree well with literature [23,25], that is, the improvement of system performance mainly benefits from the temperature glide in the condenser. When the heat source inlet temperature rises to 463.15 K, butane have the highest overall exergy efficiency. As the heat source inlet temperature increases further, the mass fraction corresponding to the maximum overall exergy efficiency moves toward the side of the higher critical temperature component, and eventually moves to pentane. This results declare that the relative value of the heat source inlet temperature and the critical temperature exhibits more significant influence on the cycle performance than the condensation

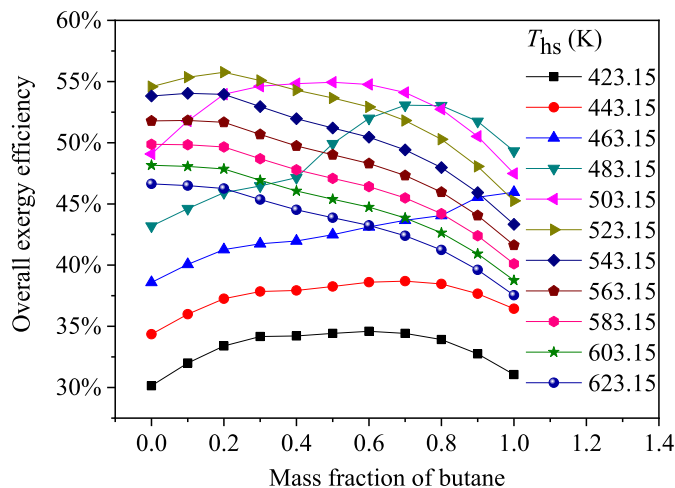


Fig. 3. Overall exergy efficiency of the ORC using butane/pentane at different heat source inlet temperature.

temperature glide. Consequently, matching the mixture with the heat source should be firstly satisfied for the selection of the working fluid.

The exergy distribution of the ORC system using butane/pentane (0.8/0.2) is calculated to get a deep understanding of the effect of the heat source inlet temperature on the system performance, as shown in Fig. 4. It can be seen that the overall exergy efficiency increases firstly and then decreases slowly, i.e., there exists an optimal relative value of the heat source inlet temperature and the critical temperature corresponding to the maximum overall exergy efficiency. Fig. 5 shows the cycle T - s diagram at the heat source inlet temperature of 443.15 K, 483.15 K and 523.15 K in order to explain the variation of the exergy distribution presented in Fig. 4. When the heat source inlet temperature is below 483.15 K, the exergy loss coefficient in the evaporator and heat source decreases with the increase in the heat source inlet temperature, as plotted in Fig. 4. At this state, the evaporator pinch point is located in the bubble point, as shown in Fig. 5(a). The large temperature difference in the evaporator results in large heat transfer exergy loss, and the high heat source outlet temperature leads to the large heat source exergy loss. With the increase of the heat source inlet temperature, the evaporation section is reduced slowly, leading to the gradual reduction of exergy loss in the evaporator and the heat source. At the heat source inlet temperature of 483.15 K, the optimal evaporation pressure is the highest pressure $0.9P_{\text{cri}}$ and the pinch point moves from the bubble point to the preheating section, as presented in Fig. 5(b). The evaporation section is reduced to a minimum so that the temperature rise of the working fluid can better match the temperature fall of the heat source in the preheating section, leading to the minimum exergy loss in the evaporator. In addition, the reduction of the heat source outlet temperature brings about the lower heat source exergy loss. As a result, the ORC system has the maximum overall exergy efficiency. Furthermore, when the heat source inlet temperature is above 483.15 K, the optimal evaporator pressure is still $0.9 P_{\text{cri}}$ and the pinch point position moves to the exit of the evaporator, as shown in Fig. 5(c). The heat source outlet temperature decreases to the lowest and remains constant, while the heat source inlet exergy increases persistently, leading to the gradual decrease of the exergy loss coefficient of the heat source. However, since the temperature rise curve of the working fluid remains constant, the increase of the heat source inlet temperature results in the larger exergy loss in the evaporator, reducing the overall exergy efficiency.

More working fluids are calculated in order to explore the correlation between the heat source inlet temperature and the mixture critical temperature. Mixtures in Table 2 with a series of concentration are used in the thermodynamic analysis. The difference between adjacent critical temperature is 0–6 K. The overall exergy efficiency when using these working fluids for different heat source inlet temperatures is shown in Fig. 6. It can be found that, for the specific heat source inlet temperature, the overall exergy efficiency first increases sharply and then decreases gradually. There exists an optimal critical temperature corresponding to the maximum overall exergy efficiency. Besides, in the range of critical temperature 507.82 K–594.55 K, three mixture working fluid are used: hexane/heptane (T_{cri} from 507.82 K to 540.13 K), heptane/octane (T_{cri} from 540.13 K to 569.32 K), octane/nonane (T_{cri} from 569.32 K to 594.55 K), as listed Table 2. There is no overlap in the range of their critical temperature. With the increase in their concentration, the condensation temperature glide can improve the overall exergy efficiency. Consequently, the periodic bumps of the overall exergy efficiency can be seen from Fig. 6.

3.1.2. Effect of the pinch temperature difference in the evaporator

Since the pinch temperature difference influences the

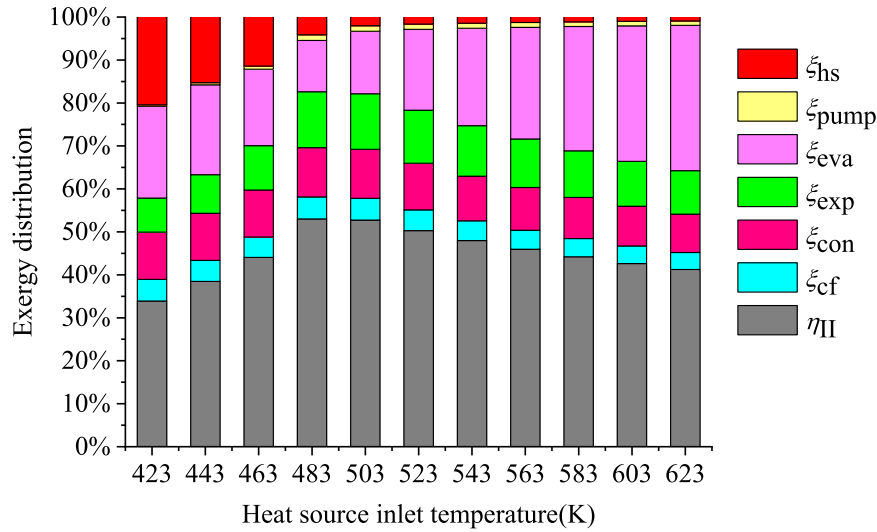


Fig. 4. Exergy distribution of the ORC using butane/pentane(0.8/0.2) at different heat source inlet temperature.

irreversibility of the heat transfer process, its effect on the selection of working fluids is studied. The cycle performance with pinch temperature difference of 10 K, 20 K and 30 K in the evaporator is calculated under different heat source inlet temperatures, and the results are summarized in Table 4. It can be seen that, with the increase of the pinch temperature difference, the mass flow rate of the working fluids, the net work output and the system thermal efficiency remain constant if the temperature difference ($T_{hs} - T_{p,eva}$) is kept unchanged. Due to the increase in the heat source inlet temperature, the higher \dot{E}_{hs} leads to the lower overall exergy efficiency. Results in Table 4 can be explained by the temperature match shown in Fig. 7. When ($T_{hs} - T_{p,eva}$) stays the same, the increase of $T_{p,eva}$ just make the temperature curve of the heat source shift up to match it. The heat absorbed by the working fluids and the cycle configuration of the working fluid stay invariant. Thus, the mass flow rate, the net work output and the thermal efficiency are unchanged. And the optimal working fluid also stays the same according to Eq. (18), which leads to the same optimal critical temperature. The increase in pinch temperature difference leads to the increase in the exergy loss of the evaporator and the decrease in the overall exergy efficiency. Since it is just a change of the thermodynamic cycle configuration, the effect of ($T_{hs} - T_{p,eva}$) on other working fluid is the same. Results in Table 4 and Fig. 7 indicate that the optimal mixture critical temperature T_{cri}^* should be correlated with ($T_{hs} - T_{p,eva}$). And ($T_{hs} - T_{p,eva}$) indicates the modified heat sources inlet temperature considering the irreversible loss during the heat transfer in the evaporator.

3.1.3. The first correlation of the selection criteria

As described in section 3.1.1, mixtures in Table 2 with the concentration step of 0.2 are used in the thermodynamic analysis to select the suitable working fluids for the heat source inlet temperature varying from 423.15 K to 623.15 K. The pinch temperature difference in the evaporator is set to 10 K. The selected working fluids are listed in Table 5 and shown in Fig. 8 represented by the black dots.

Apparently, for the black dots, a linear fitting can be applied, and the obtained correlation is:

$$T_{hs} - T_{p,eva} = 1.182T_{cri}^* - 39.244 \text{ (K)} \quad (19)$$

Where T_{hs} and $T_{p,eva}$ are known or given. The critical

temperature T_{cri}^* of the suitable mixture can be easily calculated by Eq. (19).

Thermodynamic analysis based on the mixtures in Table 3 are carried out to validate Eq. (19). Results are listed in Table 6 and shown in Fig. 8 where the halohydrocarbon mixtures with relatively precise thermophysical properties are marked in red and those without mixture experiment data are in blue. The properties of mixtures marked in blue were obtained according to the recommended mixing rules in the software REFPROP 9.0. It can be seen that the selected halohydrocarbon mixtures agree well with the linear relationship Eq. (19). The blue dot is slightly lower may due to inaccurate thermophysical properties.

3.2. The match between the working fluids and the cooling fluid

According to Eq. (19), the same critical temperature can be achieved by adjusting the mixture concentration for different components. In this case, the further improvement of the system performance relies on the optimization of the temperature match in the condenser. In this section, the correlation evaluating the temperature match in the condenser is explored and verified. It is also used as the second correlation of the selection criteria.

3.2.1. The second correlation of the selection criteria

Fig. 9 shows the ideal temperature match between the working fluids and the cooling fluid for two cases: the working fluids are saturated and subcooled liquid at the exit of the condenser, respectively. $\Delta T_{wf,con}$ is the condensation temperature glide. The overall temperature rise of the cooling fluid is $\Delta T_{cf} = \Delta T_{cf,sub} + \Delta T_{cf,con} + \Delta T_{cf,pre}$. $\Delta T_{cf,sub}$, $\Delta T_{cf,con}$ and $\Delta T_{cf,pre}$ are the temperature rise of the cooling fluid at subcooling section, condensation section and precooling section, respectively. In Fig. 9(a), the working fluids are saturated at the exit of the condenser. In this case, the ideal temperature match can be obtained when the temperature curve slope of the working fluids is the same as that of the cooling fluid in the condensation section. At this state, the temperature difference between the hot and cold fluids is equal to the pinch temperature difference everywhere:

$$\Delta T_{wf,con}^* = \Delta T_{cf,con} \quad (20)$$

In Fig. 9(b), the working fluids are subcooled liquid at the exit of

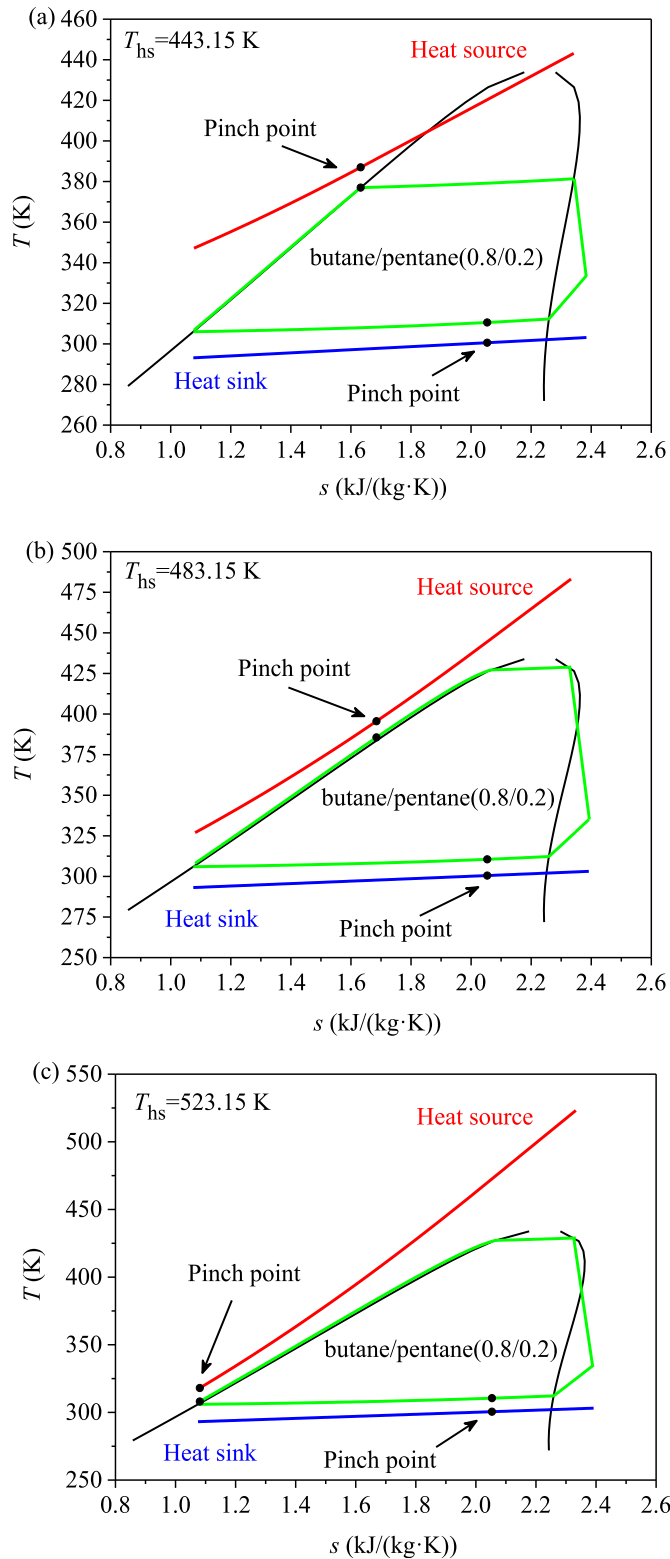


Fig. 5. T-s diagram of the ORC using butane/pentane(0.8/0.2) for (a) $T_{hs} = 443.15$ K, (b) $T_{hs} = 483.15$ K and (c) $T_{hs} = 523.15$ K.

the condenser. If ΔT_{wf_con} stays the same, the pinch point will move to the exit of the condenser so that the temperature curve of the working fluids has to move upward, represented by the red dash line. To improve the temperature match, ΔT_{wf_con} should be

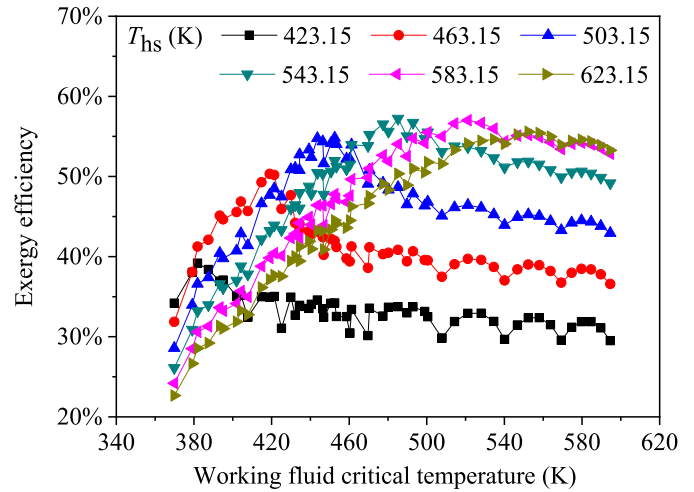


Fig. 6. Overall exergy efficiency of the ORC using different alkane mixtures at different heat source inlet temperature.

reduced until the temperature difference in the dew point is also equal to the pinch temperature difference, as shown in the red solid line. And the temperature match is:

$$\Delta T_{wf_con}^* + \Delta T_{sub} = \Delta T_{cf_con} + \Delta T_{cf_sub} \quad (21)$$

When $\Delta T_{sub} = 0$ and $\Delta T_{cf_sub} = 0$, Eq. (21) becomes Eq. (20).

For most of the working fluids, the heat flux in the precooling section is far less than that in the subcooling and condensation sections. Substituting $\Delta T_{cf} \approx \Delta T_{cf_sub} + \Delta T_{cf_con}$ into Eq. (21), we get:

$$\Delta T_{wf_con}^* = \Delta T_{cf} - \Delta T_{sub} \quad (22)$$

where ΔT_{cf} and ΔT_{sub} are both known. Consequently, the optimal condensation temperature glide can be determined by Eq. (22).

It is noted that when the mixture's slope reciprocal of the saturated vapor curve $(ds/dT)_{sv}$ is large or the heat source inlet temperature is quite high, the superheat degree at the condenser inlet will also high. In this case, ΔT_{cf_pre} can not be ignored compared with $\Delta T_{cf_sub} + \Delta T_{cf_con}$. Consequently, ΔT_{cf} should be reduced properly in Eq. (22).

3.2.2. Verification of the second correlation

As discussed in Section 3.1, for the butane/pentane mixture, the improvement of the overall exergy efficiency is mainly attributed to the condensation temperature glide in the condenser when the heat source inlet temperature is low (423.15 K and 443.15 K). Eq. (22) should be further verified. consequently, in the case of $\Delta T_{sup} = 0$ K, the overall exergy efficiency for butane/pentane with different ΔT_{sub} at the heat source inlet temperature of 423.15 K is calculated and shown in Fig. 10. The brown solid line and blue dash line represent the value on the left and right side of Eq. (22), respectively. The intersections of these two lines represent the optimal mass fraction satisfying Eq. (22). It can be seen that the maximum overall exergy efficiency appears much close to the intersections, which implies that the optimal temperature match in the condenser can be accurately described by Eq. (22).

Results of the thermodynamic analysis show that the change of the exergy losses of the expander, pump and cooling fluid is negligible compared with that of the heat source, evaporator and condenser. Thus only the variations of ξ_{hs} , ξ_{eva} and ξ_{con} with the mixture concentration are presented in Fig. 11 to explain the trends

Table 4
Cycle performance using butane/pentane for the same ($T_{hs} - T_{p_eva}$).

	$T_{hs}(K)$	$T_{p_eva}(K)$	$\dot{m}_{wf}(kg/s)$	$\dot{W}_{net}(kW)$	$\eta_{II}(\%)$	$\eta_{II}(\%)$
pentane/hexane(0.2/0.8)	483.15	10	2.66	190.57	13.68	43.05
	493.15	20	2.64	190.85	13.78	39.46
	503.15	30	2.64	191.22	13.79	36.35
pentane/hexane(0.8/0.2)	483.15	10	2.72	196.4	14.00	44.37
	493.15	20	2.72	196.76	14.01	40.68
	503.15	30	2.72	197.08	14.01	37.47
butane/pentane (0.2/0.8)	483.15	10	2.78	203.24	14.08	45.92
	493.15	20	2.78	203.56	14.09	42.09
	503.15	30	2.76	203.88	14.19	38.76
butane/pentane (0.8/0.2)	483.15	10	3.31	234.72	14.80	53.03
	493.15	20	3.32	235.01	14.80	48.59
	503.15	30	3.32	235.39	14.80	44.75
propane/butane (0.2/0.8)	483.15	10	3.80	217.84	12.86	49.22
	493.15	20	3.81	218.17	12.86	45.11
	503.15	30	3.81	218.44	12.86	41.53
propane/butane (0.8/0.2)	483.15	10	4.19	171.54	10.25	38.75
	493.15	20	4.2	171.75	10.25	35.51
	503.15	30	4.2	171.97	10.25	32.69

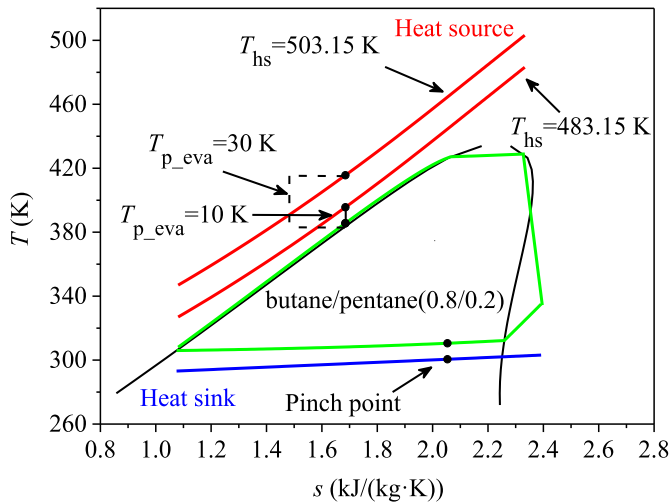


Fig. 7. T - s diagram of the ORC using butane/pentane(0.8/0.2) for the same ($T_{hs} - T_{p_eva}$).

Table 5
Optimal working fluids used for data fitting.

$(T_{hs} - T_{p_eva})(K)$	Working fluids	$T_{cri}(K)$	$\eta_{II}(\%)$
413.15	propane/butane (0.8/0.2)	381.9	39.17
433.15	propane/isobutane (0.4/0.6)	395.05	44.54
453.15	isobutene/isopentane(0.8/0.2)	419.03	50.32
473.15	butane/pentane(0.8/0.2)	434.5	53.03
493.15	butane/pentane(0.4/0.6)	452.58	54.83
513.15	Isopentane/hexane(0.8/0.2)	470.47	56.03
533.15	pentane/hexane(0.6/0.4)	485.22	57.23
553.15	butane/pentane(0.2/0.8)	500.49	56.87
573.15	hexane/heptane(0.6/0.4)	521.16	57.01
593.15	hexane/heptane(0.4/0.6)	528.05	56.02
613.15	heptane/octane(0.6/0.4)	552.32	55.58

of the overall exergy efficiency profiles. It is seen that ξ_{hs} and ξ_{con} show the similar varying trend with the mixture concentration while ξ_{eva} exhibits the reverse trend. When ΔT_{wf_con} is lower than the optimal condensation temperature glide calculated by Eq. (22), the increase in ΔT_{wf_con} leads to the decrease of the mixture temperature at the outlet of the condenser and the optimization of temperature match in the condenser. Consequently, ξ_{hs} and ξ_{con} are

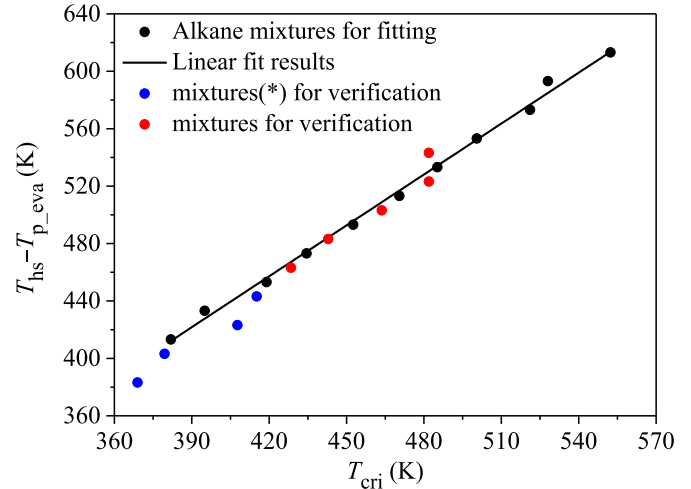


Fig. 8. Linear fitting of the temperature match in the evaporator ($T_{hs} - T_{p_eva}$) with T_{cri} .

Table 6
Optimal working fluids used for verification.

$(T_{hs} - T_{p_eva})(K)$	Working fluids	$T_{cri}(K)$	$\eta_{II}(\%)$
383.15	R218/R236fa (0.6/0.4)	368.99	35.32
403.15	R218/R236fa (0.4/0.6)	379.49	41.48
423.15	RC318/R245fa (0.6/0.4)	407.72	44.91
443.15	RC318/R245fa (0.4/0.6)	415.19	49.24
463.15	R114/R113 (0.9/0.1)	428.45	52.17
483.15	R114/R113 (0.7/0.3)	442.94	54.22
503.15	R114/R113 (0.4/0.6)	463.67	54.41
523.15	R114/R113 (0.1/0.9)	481.93	57.28
543.15	R114/R113 (0.1/0.9)	481.93	57.11

Notes: Blue represents the halohydrocarbon mixtures without mixture experiment data. Red represents the halohydrocarbon mixtures with relatively precise thermophysical properties.

reduced. Note that the mixture critical temperature and the fluid mass flow rate also change with the mixture concentration. The combine effects of ΔT_{wf_con} , the critical temperature and the mass flow rate on the temperature match in the evaporator lead to the increase in ξ_{eva} with the mass fraction of butane varying from 0 or 1.0 to the optimal mass fraction. Generally, the variation of ξ_{hs} and ξ_{con} dominates the change of η_{II} . Therefore, the local maximum

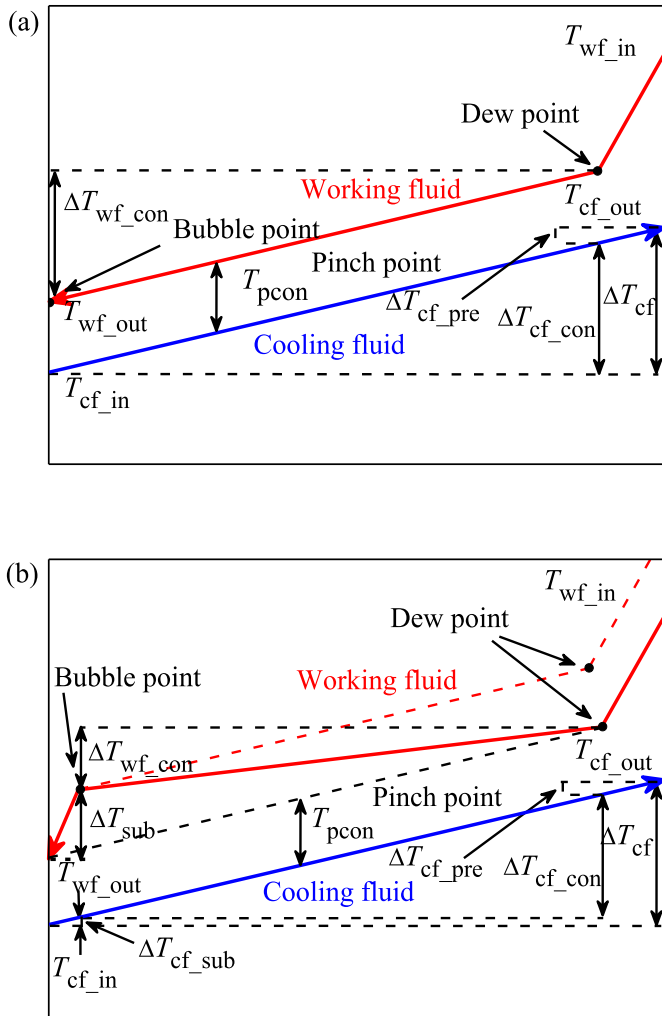


Fig. 9. Ideal temperature match between the working fluid and cooling fluid in the condenser for (a) without subcooling and (b) subcooling.

overall exergy efficiency appears at the temperature glide close to $\Delta T_{wf_con}^*$ calculated by Eq. (22).

The inlet superheat degree of the expander influences that of the condenser. In the case of $\Delta T_{sub} = 0$ K, taking butane/pentane as an example, we studied the effect of inlet superheat degree of the expander ΔT_{sup} on the cycle performance and plotted the results in Fig. 12. ΔT_{sup} in practice is usually controlled below 10 K. Thus, three cases with ΔT_{sup} of 0, 5 and 10 K was calculated. It can be found that the increase of ΔT_{sup} decreases the overall exergy efficiency due to the decrease in the system shaft power. However, the change of ΔT_{sup} does not affect the optimal mass fraction of butane because the temperature rise of the cooling fluid in the precooling section is much lower relative to the overall temperature rise. As a result, the optimal temperature condition in the condenser is still accordance with Eq. (22).

3.2.3. Determination method of the optimal mixing fraction

Since ΔT_{cf} and ΔT_{sub} in Eq. (22) are known, the key issue of the mixture selection is to determine the mixture temperature glide in the condenser without thermodynamic calculation. As described in section 3.2.1, for the ideal temperature match, the heat transfer temperature difference at the exit of the condenser is equal to the pinch temperature difference. Thereby the bubble point

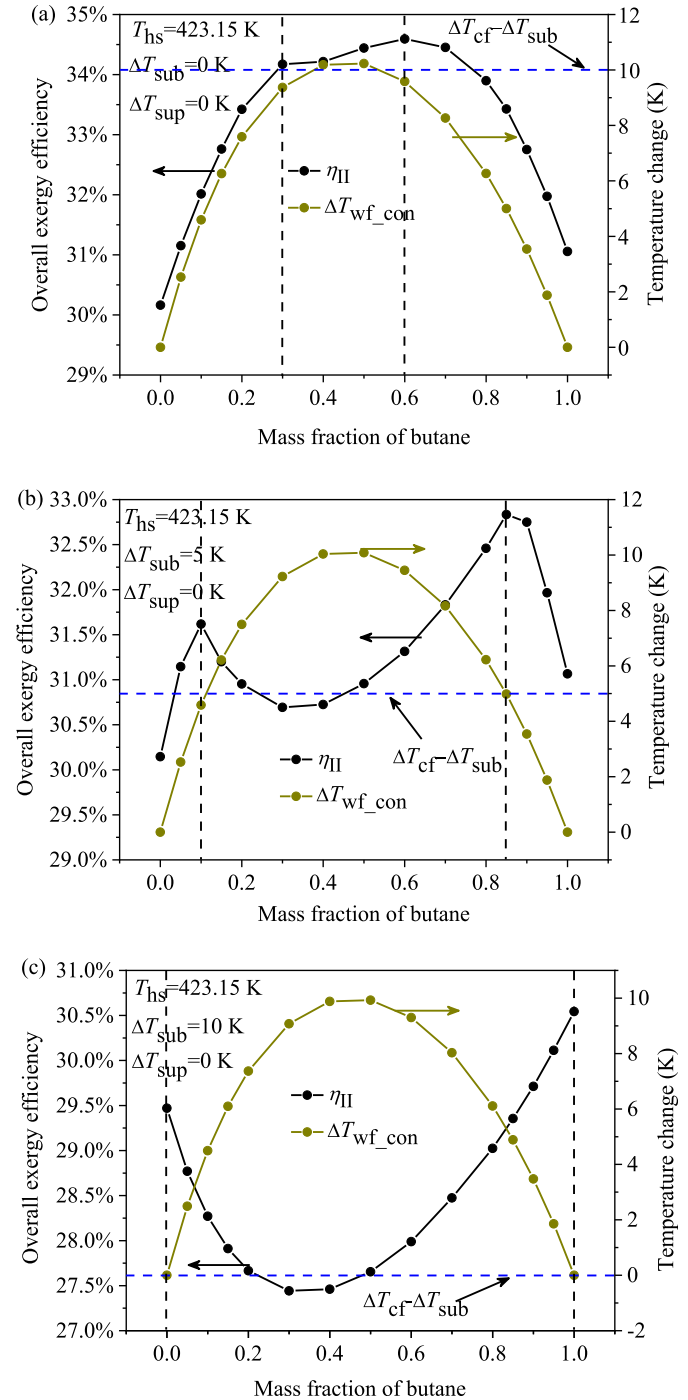


Fig. 10. Overall exergy efficiency of the ORC using butane/pentane for (a) $\Delta T_{sub} = 0$ K, (b) $\Delta T_{sub} = 5$ K and (c) $\Delta T_{sub} = 10$ K.

temperature T_{bubble} can be given as:

$$T_{bubble} = T_{cf_in} + T_{p_con} + \Delta T_{sub} \quad (23)$$

where T_{cf_in} , T_{p_con} and ΔT_{sub} are all known. Based on the thermophysical property database Refprop, the condensation pressure and the dew point temperature for a fixed mixture concentration can be easily obtained from the built-in functions:

$$P_{con} = f(T_{bubble}, x) \quad (24)$$

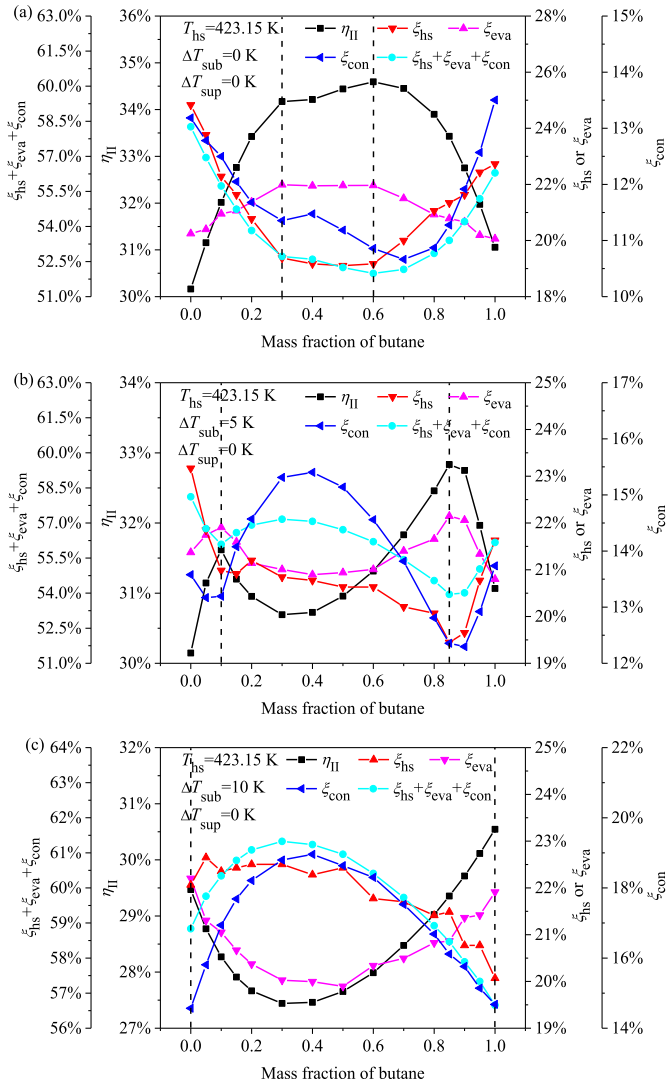


Fig. 11. Exergy loss of the ORC using butane/pentane for (a) $\Delta T_{sub}=0$ K, (b) $\Delta T_{sub}=5$ K and (c) $\Delta T_{sub}=10$ K.

$$T_{dew} = g(P_{con}, x) \quad (25)$$

Thus, the condensation temperature glide can be acquired by

$$\Delta T_{wf_con} = T_{dew} - T_{bubble} \quad (26)$$

3.3. Screening criteria of the working fluids and verification

3.3.1. Steps of using the screening criteria

Eqs. (19) and (22) constitute the thermodynamic selection criteria of the mixture working fluid. And the criteria are obtained according to the optimization objective of the overall exergy efficiency. In terms of the selection of working fluids, the system cost, environment indicators, toxicity and flammability should also be considered [20]. Consequently, the purpose of using the present thermodynamic selection criteria is to easily and rapidly filter out several mixtures with superior thermodynamic performance rather than the solely best mixture. Due to the discontinuous variation of the condensation temperature glide, a temperature range is added to Eq. (22):

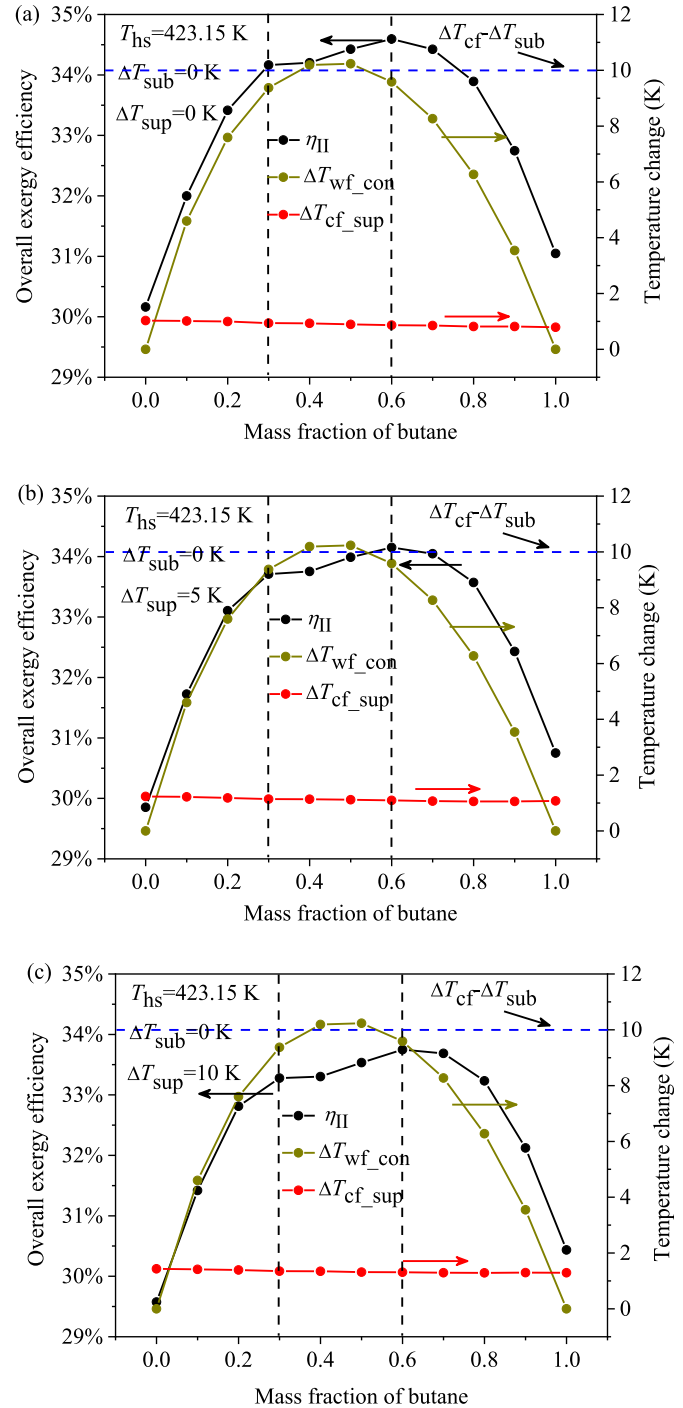


Fig. 12. Overall exergy efficiency of the ORC using butane/pentane for (a) $\Delta T_{sub}=0$ K, (b) $\Delta T_{sub}=5$ K and (c) $\Delta T_{sub}=10$ K.

$$\Delta T_{wf_con}^* = (\Delta T_{cf} - \Delta T_{sub}) \pm \alpha K \quad (27)$$

where α can be determined by the number of mixtures which can offer the temperature glide close to $\Delta T_{wf_con}^*$ in Eq. (22). And $\alpha = 2$ K is proposed in this paper.

Based on the above discussion, the mixture screening steps are summarized below:

Step 1: Determination of the mixture critical temperature and concentration. For a specific heat source inlet temperature,

Table 7
Condensation temperature glide of working fluids used for selection ($T_{\text{cri}}^* = 382.74$ K).

Working fluid	$\Delta T_{\text{sub}} = 0$ K			$\Delta T_{\text{sub}} = 5$ K		
	predicted $\Delta T_{\text{wf_con}}^r$ (K)	$\Delta T_{\text{wf_con}}^r$ (K)	relative error(%)	predicted $\Delta T_{\text{wf_con}}^r$ (K)	$\Delta T_{\text{wf_con}}^r$ (K)	relative error(%)
propane/RC318 (0.0882)	6.71	6.56	2.29	6.42	6.42	0.00
propane/isobutene (0.717)	5.44	5.33	2.06	5.31	5.31	0.00
propane/R114 (0.4201)	10.47	10.40	0.67	10.13	10.13	0.00
propane/neopentane(0.7991)	10.39	10.30	0.87	10.13	10.13	0.00
propane/butane (0.7855)	8.16	8.06	1.24	7.93	7.93	0.00
propylene/RC318 (0.0602)	7.86	7.78	1.03	7.53	7.53	0.00
propylene/isobutane (0.6607)	7.43	7.36	0.95	7.28	7.28	0.00
propylene/R236ea (0.3073)	16.33	16.25	0.49	15.47	15.47	0.00
propylene/R114 (0.3517)	14.98	14.98	0.00	14.52	14.51	0.07
propylene/neopentane(0.6162)	18.63	18.62	0.05	18.20	18.20	0.00
propylene/butane (0.7634)	12.13	12.10	0.25	11.82	11.82	0.00
propylene/R245ca (0.5234)	19.53	19.33	1.03	18.34	18.34	0.00
R115/RC318 (0.1281)	5.12	4.96	3.23	4.91	4.91	0.00
R115/R236fa (0.3445)	12.43	12.43	0.00	11.90	11.90	0.00
R115/isobutene (0.6921)	7.36	7.29	0.96	7.21	7.21	0.00
R115/R236ea (0.5045)	15.71	15.71	0.00	15.05	15.05	0.00
R115/R114 (0.594)	13.09	13.09	0.00	12.76	12.76	0.00
R115/propyne (0.594)	1.93	1.78	8.43	1.83	1.77	3.39
R115/R245fa (0.6333)	18.75	18.74	0.05	17.93	17.92	0.06
R115/neopentane(0.7865)	17.06	17.06	0.00	16.71	16.71	0.00
R115/butane (0.7917)	11.53	11.53	0.00	11.27	11.27	0.00
R115/R245ca (0.7159)	22.59	22.57	0.09	21.66	21.66	0.00
R134a/R236fa (0.5467)	4.17	4.04	3.22	4.06	4.04	0.50
R134a/R236ea (0.7003)	5.11	4.98	2.61	4.97	4.97	0.00
R134a/propyne (0.8543)	0.01	0.01	0.00	0.01	0.01	0.00
R134a/R245fa (0.7985)	6.42	6.27	2.39	6.21	6.21	0.00
R134a/R245ca (0.8526)	8.08	7.92	2.02	7.82	7.82	0.00
R218/R114 (0.5128)	13.18	13.18	0.00	12.92	12.92	0.00
R218/R236ea (0.4933)	15.49	15.49	0.00	14.93	14.93	0.00
R218/R236fa (0.3345)	10.74	10.74	0.00	10.32	10.32	0.00
R218/RC318 (0.1232)	4.32	4.18	3.35	4.16	4.16	0.00
R218/propyne (0.7096)	1.30	1.21	7.44	1.25	1.21	3.31
R218/R245fa (0.6229)	19.74	19.74	0.00	19.01	19.01	0.00
R218/neopentane(0.7789)	17.88	17.88	0.00	17.58	17.58	0.00
R218/butane (0.7843)	11.54	11.54	0.00	11.33	11.33	0.00
R218/R245ca (0.7068)	24.61	24.61	0.00	23.80	23.80	0.00
R227ea/R236fa (0.6862)	1.05	0.98	7.14	1.01	0.98	3.06
R227ea/isobutene (0.6065)	4.49	4.48	0.22	4.48	4.48	0.00
R227ea/R236ea (0.809)	2.29	2.18	5.05	2.21	2.17	1.84
R227ea/R114 (0.8208)	1.01	1.01	0.00	1.01	1.01	0.00
R227ea/propyne (0.914)	0.24	0.21	14.29	0.22	0.21	4.76
R227ea/R245fa (0.8778)	2.37	2.22	6.76	2.27	2.22	2.25
R227ea/butane (0.9405)	0.38	0.41	-7.32	0.40	0.41	-2.44
R227ea/R245ca (0.913)	3.93	3.76	4.52	3.78	3.76	0.53
R1234yf/RC318 (0.1776)	4.14	4.00	3.50	4.00	4.00	0.00
R1234yf/R236fa (0.4357)	5.78	5.58	3.58	5.53	5.53	0.00
R1234yf/isobutene (0.7676)	3.15	3.14	0.32	3.14	3.14	0.00
R1234yf/R236ea (0.5994)	6.69	6.50	2.92	6.38	6.38	0.00
R1234yf/R114 (0.6179)	7.53	7.48	0.67	7.39	7.39	0.00
R1234yf/propyne (0.7897)	0.15	0.13	15.38	0.14	0.13	7.69
R1234yf/R245fa (0.7173)	8.23	8.03	2.49	7.83	7.83	0.00
R1234yf/neopentane(0.8441)	10.30	10.28	0.19	10.19	10.19	0.00
R1234yf/butane (0.8481)	6.02	5.96	1.01	5.93	5.93	0.00
R1234yf/R245ca (0.7874)	10.77	10.60	1.60	10.29	10.29	0.00

the optimal critical temperature of the mixture T_{cri}^* is calculated by Eq. (19). Then, pure working fluids with critical temperature above and below T_{cri}^* are selected to form the binary zeotropic mixture. By adjusting their concentration, a series of mixtures with T_{cri}^* can be obtained.

Step 2: Excluding the ‘wet’ mixture. On the thermodynamic point of view, working fluids can be categorized into “dry”, “wet” and “isentropic” types according to their saturated vapor curve in the T - s diagram. Since the slope of mixture saturated vapor curve varies with the mixing fraction nonlinearly, the mixtures can have different characteristics of saturated vapor curve through the mixing fraction regulation [52]. The mixtures with the obvious “wet” behavior should be excluded according to their saturated vapor curves in the T - s diagram because the

large superheat degree at the expander inlet will reduce the cycle performance [53,54]. This will be illustrated in section 3.3.2.

Step 3: Selecting mixtures with proper condensation temperature glide. For a specific cooling fluid inlet temperature, the condensation temperature glide of obtained mixtures in step 2 can be acquired from the property database according to Eqs. (23)–(26). Then, the suitable mixtures can be selected according to Eq. (27).

3.3.2. Application and verification of the selection criteria

Since the present selection criteria are only related to thermodynamic properties of the working fluids, it is also applicable to the

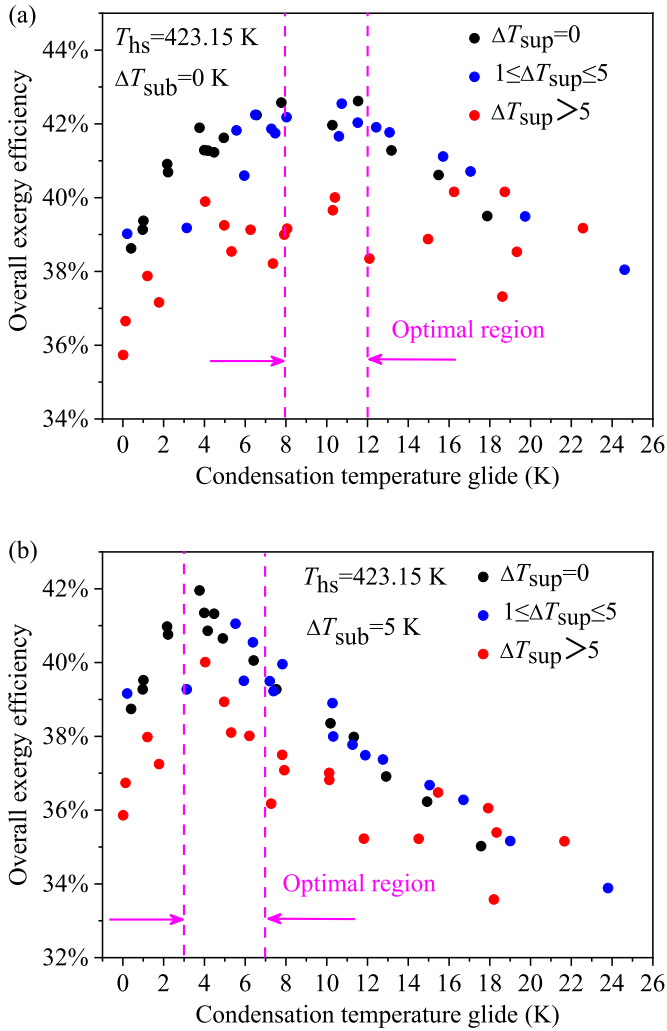


Fig. 13. Selected mixture working fluids for (a) $\Delta T_{sub} = 0$ K and (b) $\Delta T_{sub} = 5$ K.

multicomponent mixtures. In this section, the criteria are applied to binary mixtures to verify the criteria. The heat source inlet temperature is fixed at 423.15 K and there is no limitation to the outlet temperature. The subcooling degree at the exit of the condenser is 0 K and 5 K, respectively. Other operation conditions are listed in Table 1.

The optimal critical temperature calculated by Eq. (19) is 382.74 K. Seven pure fluids with critical temperature lower than 382.74 K and ten pure fluids with critical temperature higher than 382.74 K are randomly chosen to form mixtures whose thermodynamic properties can be acquired from Refprop. The mixture concentration is identified to satisfy the optimal critical temperature 382.74 K, as listed in Table 7.

In these calculation cases, the “wet” mixtures are not excluded to analyze the effect of the superheat degree on the selection of mixture working fluid. The condensation temperature glide of the

mixtures is predicted by the method described in step 3 in section 3.3.1. And the results are listed in Table 7. For the two cases: $\Delta T_{sub} = 0$ K and $\Delta T_{sub} = 5$ K, $\Delta T_{wf_con}^*$ in Eq. (27) is in the range of 8–12 K and 3–7 K ($\alpha = 2$ K), respectively. Thus, the optimal thermodynamic performance mixtures are screened based on the temperature range.

Since the selection criteria and the method to predict the condensation temperature glide need to be further verified, the thermodynamic calculation is performed for the mixtures under $\Delta T_{sub} = 0$ K and $\Delta T_{sub} = 5$ K, respectively. The condensation temperature glide calculated in the thermodynamic analysis is also listed in Table 7 and compared with the prediction value in Eq. (26). It is seen that the difference between prediction and calculation value is quite small and most of relative errors are less than 5%, which demonstrates the feasibility of selecting mixtures by the predicted value without massive calculation. The distribution of overall exergy efficiency varying with the condensation temperature glide is shown in Fig. 13. It is found that the mixtures in the ‘optimal region’ can offer relatively higher overall exergy efficiency, indicating the validity of the criteria. Since the evaporation pressure of the mixtures identified by Eq. (19) is usually $0.9P_{cri}$, the superheat degree for the “wet” working fluids should be large enough (usually above 5 K) to avoid the two phase region at the exit of the expander. It can be seen from Fig. 13 that the overall exergy efficiency of the ‘wet’ mixtures with the larger superheat degree ($\Delta T_{sup} > 5$ K) is lower than that of other mixtures. This is why the step 2 in the screening criteria needs to be implemented to eliminate the “wet” working fluids according to the characteristics of their saturated vapor curve in the T - s diagram.

Additionally, after the first selection step are satisfied (T_{cri}^* are achieved), for the mixtures with smaller or without superheat degree, performance of the selected mixture working fluid is compared with the mixtures whose condensation temperature glide is closest to 0 to demonstrate the improvement of the cycle performance attributed to the better temperature match, as listed in Table 8. It can be found that the overall exergy efficiency is improved by 9.23% and 7.12% for the cases $\Delta T_{sub} = 0$ K and $\Delta T_{sub} = 5$ K, respectively.

4. Conclusions

Although using zeotropic mixtures in the ORC system can improve its performance, the selection of the mixture working fluid is still a great challenge due to the lack of selection criteria. The present work proposes a thermodynamic selection criteria for zeotropic mixtures based on the exergy analysis of the subcritical ORC. The temperature match between the working fluids and the heat source/sink are analyzed. The steps of using this selection criteria and a case study to validate it are also illustrated. The main conclusions are summarized as follows:

- (1) The proposed selection criteria for zeotropic mixture consist of two correlations: $T_{hs} - T_{p_eva} = 1.182T_{cri}^* - 39.244$ (K) and $\Delta T_{wf_con}^* = \Delta T_{cf} - \Delta T_{sub}$, which describe the working fluids optimal temperature match with the heat source and

Table 8
Cycle performance improvement by mixtures with $T_{cri}^* = 382.74$ K.

Subcooling degree	Working fluids	ΔT_{wf_con} (K)	η_{II} (%)	η_{II} improvement rate
$\Delta T_{sub} = 0$ K	R227ea/propyne (0.914)	0.21	39.02	–
	R218/butane (0.7843)	11.54	42.62	9.23%
$\Delta T_{sub} = 5$ K	R227ea/propyne (0.914)	0.21	39.16	–
	R227ea/R245ca (0.913)	3.76	41.95	7.12%

the cooling fluid, respectively. The mixture composition can be directly determined according to the thermophysical properties of working fluids without massive thermodynamic calculation.

- (2) For the heat source without limit to the outlet temperature, the improvement of the temperature match in the evaporator exhibits more significant influence on the cycle performance than that in the condenser because the evaporator pinch point moves from the bubble point to the preheating section. Consequently, the match condition with the heat source should be firstly satisfied.
- (3) For the temperature glide in the condenser, its effect on the improvement of the overall exergy efficiency is mainly attributed to combine effects of the increase in the heat source utilization, the decrease in the condenser exergy loss and the increase in the evaporator exergy loss. And the influence of the former two on the overall exergy efficiency is greater than the latter.
- (4) Similar to the principles of using pure working fluid, the 'wet' working fluids have relatively lower cycle performance compare to 'dry' and 'isentropic' ones when using zeotropic mixtures in the ORC system. Thus, the 'wet' mixtures are not recommended in the present selection criteria.

Acknowledgements

This work was supported by the National Natural Science Foundation of China (No. 51776064 and No.) and the Fundamental Research Funds for the Central Universities (No. 2018MS018).

Nomenclature

List of symbols

\dot{E}	exergy flow rate, kW
h	specific enthalpy, kJ/kg
\dot{i}	exergy loss rate, kW
\dot{m}	mass flow rate, kg/s
P	pressure, kPa
\dot{Q}	heat transfer rate, kW
s	specific entropy, kJ/(kg·K)
T	temperature, K
\dot{W}	power, kW
η	efficiency
Δ	change or difference
ξ	exergy loss coefficient

Abbreviations

ORC	organic Rankine cycle
-----	-----------------------

Greek letters

η	efficiency
Δ	change or difference
ξ	exergy loss coefficient

Subscripts and superscripts

0	reference environment state
I	thermodynamic first law
II	thermodynamic second law
abs	absorption
bubble	bubble point
cf	cooling fluid
con	condensation or condenser
cri	critical state

eva	evaporator
exp	expander
hs	heat source.
in	inlet
net	net output
out	outlet
p	pinch point
pre	precooling or preheating section
pump	pump
rel	release
sub	subcooling degree
sup	superheat degree
wf	working fluid
*	optimal value

References

- [1] Hung TC, Shai TY, Wang SK. A review of organic Rankine cycles (ORCs) for the recovery of low grade waste heat. *Energy* 1997;22(7):661–7.
- [2] Hung T-C. Waste heat recovery of organic Rankine cycle using dry fluids. *Energy Convers Manag* 2001;42:539–53.
- [3] Clemente S, Micheli D, Reini M, Taccani R. Energy efficiency analysis of Organic Rankine Cycles with scroll expanders for cogenerative applications. *Appl Energy* 2012;97:792–801.
- [4] Miao Z, Xu J, Yang X, Zou J. Operation and performance of a low temperature organic Rankine cycle. *Appl Therm Eng* 2015;75:1065–75.
- [5] Miao Z, Xu J, Zhang K. Experimental and modeling investigation of an organic Rankine cycle system based on the scroll expander. *Energy* 2017;134:35–49.
- [6] Chen Q, Xu J, Chen H. A new design method for Organic Rankine Cycles with constraint of inlet and outlet heat Carrier fluid temperatures coupling with the heat source. *Appl Energy* 2012;98:562–73.
- [7] Modi A, Haglind F. A review of recent research on the use of zeotropic mixtures in power generation systems. *Energy Convers Manag* 2017;138:603–26.
- [8] Aljundi IH. Effect of dry hydrocarbons and critical point temperature on the efficiencies of organic Rankine cycle. *Renew Energy* 2011;36(4):1196–202.
- [9] He C, Liu C, Gao H, Xie H, Li Y, Wu S, et al. The optimal evaporation temperature and working fluids for subcritical organic Rankine cycle. *Energy* 2012;38(1):136–43.
- [10] Liu C, He C, Gao H, Xu X, Xu J. The optimal evaporation temperature of subcritical ORC based on second law efficiency for waste heat recovery. *Entropy* 2012;14(12):491–504.
- [11] Mago PJ. Exergetic evaluation of an organic Rankine cycle using medium-grade waste heat. *Energy Sources, Part A Recovery, Util Environ Eff* 2012;34(19):1768–80.
- [12] Wang D, Ling X, Peng H, Liu L, Tao L. Efficiency and optimal performance evaluation of organic Rankine cycle for low grade waste heat power generation. *Energy* 2013;50:343–52.
- [13] Ayachi F, Boulawz Ksayer E, Zoughaib A, Neveu P. ORC optimization for medium grade heat recovery. *Energy* 2014;68:47–56.
- [14] Xu J, Yu C. Critical temperature criterion for selection of working fluids for subcritical pressure Organic Rankine cycles. *Energy* 2014;74:719–33.
- [15] Hærvig J, Sørensen K, Condra TJ. Guidelines for optimal selection of working fluid for an organic Rankine cycle in relation to waste heat recovery. *Energy* 2016;96:592–602.
- [16] Vivian J, Manente G, Lazzaretto A. A general framework to select working fluid and configuration of ORCs for low-to-medium temperature heat sources. *Appl Energy* 2015;156:727–46.
- [17] Yu H, Feng X, Wang Y. A new pinch based method for simultaneous selection of working fluid and operating conditions in an ORC (Organic Rankine Cycle) recovering waste heat. *Energy* 2015;90:36–46.
- [18] Vetter C, Wiemer H-J, Kuhn D. Comparison of sub- and supercritical Organic Rankine Cycles for power generation from low-temperature/low-enthalpy geothermal wells, considering specific net power output and efficiency. *Appl Therm Eng* 2013;51(1–2):871–9.
- [19] Zhai H, An Q, Shi L. Analysis of the quantitative correlation between the heat source temperature and the critical temperature of the optimal pure working fluid for subcritical organic Rankine cycles. *Appl Therm Eng* 2016;99:383–91.
- [20] Bao J, Zhao L. A review of working fluid and expander selections for organic Rankine cycle. *Renew Sustain Energy Rev* 2013;24:325–42.
- [21] Bamorovat Abadi G, Kim KC. Investigation of organic Rankine cycles with zeotropic mixtures as a working fluid: advantages and issues. *Renew Sustain Energy Rev* 2017;73:1000–13.
- [22] Chys M, van den Broek M, Vanslambrouck B, De Paep M. Potential of zeotropic mixtures as working fluids in organic Rankine cycles. *Energy* 2012;44(1):623–32.
- [23] Heberle F, Preißinger M, Brüggemann D. Zeotropic mixtures as working fluids in Organic Rankine Cycles for low-enthalpy geothermal resources. *Renew Energy* 2012;37(1):364–70.
- [24] Liu Q, Duan Y, Yang Z. Effect of condensation temperature glide on the

- performance of organic Rankine cycles with zeotropic mixture working fluids. *Appl Energy* 2014;115:394–404.
- [25] Lecompte S, Ameel B, Ziviani D, van den Broek M, De Paepe M. Exergy analysis of zeotropic mixtures as working fluids in organic Rankine cycles. *Energy Convers Manag* 2014;85:727–39.
- [26] Li Y-R, Du M-T, Wu C-M, Wu S-Y, Liu C. Potential of organic Rankine cycle using zeotropic mixtures as working fluids for waste heat recovery. *Energy* 2014;77:509–19.
- [27] Zhou Y, Wu Y, Li F, Yu L. Performance analysis of zeotropic mixtures for the dual-loop system combined with internal combustion engine. *Energy Convers Manag* 2016;118:406–14.
- [28] Kang Z, Zhu J, Lu X, Li T, Wu X. Parametric optimization and performance analysis of zeotropic mixtures for an organic Rankine cycle driven by low-medium temperature geothermal fluids. *Appl Therm Eng* 2015;89:323–31.
- [29] Shu G, Gao Y, Tian H, Wei H, Liang X. Study of mixtures based on hydrocarbons used in ORC (Organic Rankine Cycle) for engine waste heat recovery. *Energy* 2014;74:428–38.
- [30] Song J, Gu C-w. Analysis of ORC (Organic Rankine Cycle) systems with pure hydrocarbons and mixtures of hydrocarbon and retardant for engine waste heat recovery. *Appl Therm Eng* 2015;89:693–702.
- [31] Mavrou P, Papadopoulos AI, Seferlis P, Linke P, Voutetakis S. Selection of working fluid mixtures for flexible Organic Rankine Cycles under operating variability through a systematic nonlinear sensitivity analysis approach. *Appl Therm Eng* 2015;89:1054–67.
- [32] Dong B, Xu G, Cai Y, Li H. Analysis of zeotropic mixtures used in high-temperature Organic Rankine cycle. *Energy Convers Manag* 2014;84:253–60.
- [33] Andreasen JG, Larsen U, Knudsen T, Pierobon L, Haglind F. Selection and optimization of pure and mixed working fluids for low grade heat utilization using organic Rankine cycles. *Energy* 2014;73:204–13.
- [34] Lu J, Zhang J, Chen S, Pu Y. Analysis of organic Rankine cycles using zeotropic mixtures as working fluids under different restrictive conditions. *Energy Convers Manag* 2016;126:704–16.
- [35] Satanphol K, Pridasawas W, Suphanit B. A study on optimal composition of zeotropic working fluid in an Organic Rankine Cycle (ORC) for low grade heat recovery. *Energy* 2017;123:326–39.
- [36] Heberle F, Brüggemann D. Thermo-Economic evaluation of organic Rankine cycles for geothermal power generation using zeotropic mixtures. *Energies* 2015;8(3):2097–124.
- [37] Feng Y, Hung T, Greg K, Zhang Y, Li B, Yang J. Thermoeconomic comparison between pure and mixture working fluids of organic Rankine cycles (ORCs) for low temperature waste heat recovery. *Energy Convers Manag* 2015;106:859–72.
- [38] Wu Y, Zhu Y, Yu L. Thermal and economic performance analysis of zeotropic mixtures for organic Rankine cycles. *Appl Therm Eng* 2016;96:57–63.
- [39] Xi H, Li M-J, He Y-L, Zhang Y-W. Economical evaluation and optimization of organic Rankine cycle with mixture working fluids using R245fa as flame retardant. *Appl Therm Eng* 2017;113:1056–70.
- [40] Magdalena Santos-Rodriguez M, Flores-Tlacuahuac A, Zavala VM. A stochastic optimization approach for the design of organic fluid mixtures for low-temperature heat recovery. *Appl Energy* 2017;198:145–59.
- [41] Bao J, Zhang R, Yuan T, Zhang X, Zhang N, He G. A simultaneous approach to optimize the component and composition of zeotropic mixture for power generation systems. *Energy Convers Manag* 2018;165:354–62.
- [42] Zhao L, Bao J. Thermodynamic analysis of organic Rankine cycle using zeotropic mixtures. *Appl Energy* 2014;130:748–56.
- [43] Braimakis K, Preißinger M, Brüggemann D, Karellas S, Panopoulos K. Low grade waste heat recovery with subcritical and supercritical Organic Rankine Cycle based on natural refrigerants and their binary mixtures. *Energy* 2015;88:80–92.
- [44] Zhai H, An Q, Shi L. Zeotropic mixture active design method for organic Rankine cycle. *Appl Therm Eng* 2017;129:1171–80.
- [45] DiPippo R. Second Law assessment of binary plants generating power from low-temperature geothermal fluids. *Geothermics* 2004;33(5):565–86.
- [46] Long R, Bao YJ, Huang XM, Liu W. Exergy analysis and working fluid selection of organic Rankine cycle for low grade waste heat recovery. *Energy* 2014;73:475–83.
- [47] Maraver D, Royo J, Lemort V, Quoilin S. Systematic optimization of subcritical and transcritical organic Rankine cycles (ORCs) constrained by technical parameters in multiple applications. *Appl Energy* 2014;117:11–29.
- [48] Radulovic J, Beleno Castaneda NI. On the potential of zeotropic mixtures in supercritical ORC powered by geothermal energy source. *Energy Convers Manag* 2014;88:365–71.
- [49] Miao Z, Yang X, Xu J, Zou J. Development and dynamic characteristics of an organic Rankine cycle. *Chin Sci Bull* 2014;59(33):4367–78.
- [50] Lemmon E, Huber M, McLinden M. Reference fluid thermodynamic and transport properties-refprop, standard reference database 23. National Institute of Standards and Technology; 2007., version 9.0.
- [51] Lemmon EW, Jacobsen RT. Equations of state for mixtures of R-32, R-125, R-134a, R-143a, and R-152a. *J Phys Chem Ref Data* 2002;33(2):593–620.
- [52] Su W, Zhao L, Deng S. New knowledge on the temperature-entropy saturation boundary slope of working fluids. *Energy* 2017;119:211–7.
- [53] Mago PJ, Chamra LM, Srinivasan K, Somayaji C. An examination of regenerative organic Rankine cycles using dry fluids. *Appl Therm Eng* 2008;28(8–9):998–1007.
- [54] Aghahosseini S, Dincer I. Comparative performance analysis of low-temperature Organic Rankine Cycle (ORC) using pure and zeotropic working fluids. *Appl Therm Eng* 2013;54(1):35–42.